

# Unconditional conversion between quantum particles and waves

Yoshichika Miwa<sup>1</sup>, Jun-ichi Yoshikawa<sup>1</sup>, Noriaki Iwata<sup>1</sup>, Mamoru Endo<sup>1</sup>,  
Petr Marek<sup>2</sup>, Radim Filip<sup>2</sup>, Peter van Loock<sup>3</sup> & Akira Furusawa<sup>1</sup>

<sup>1</sup>*Department of Applied Physics, School of Engineering,*

*The University of Tokyo, 7-3-1 Hongo, Bunkyo-ku, Tokyo 113-8656, Japan*

<sup>2</sup>*Department of Optics, Palacký University,*

*17. listopadu 1192/12, 772 07 Olomouc, Czech Republic*

<sup>3</sup>*Institute of Physics, Staudingerweg 7,*

*Johannes Gutenberg-Universität Mainz, 55099 Mainz, Germany*

Wave-particle duality is a basic notion of quantum mechanics, which has largely contributed to many debates on the foundations of quantum theory<sup>1–6</sup>. Besides this fundamental aspect of the wave-particle nature of quantum systems, recently, it turned out that, in order to construct more advanced and efficient protocols in quantum communication<sup>7,8</sup> and information processing<sup>9</sup>, it is also beneficial to combine continuous-wave and discrete-particle features in a so-called hybrid fashion. However, in traditional, quantum optical complementarity tests, monitoring the light waves would still happen in an effectively particle-like fashion, detecting the fields click by click<sup>10</sup>. Similarly, close-to-classical, wave-like coherent states<sup>11</sup>, as readily available from standard laser sources, or other Gaussian states generated through nonlinear optical interactions, have been so far experimentally converted into non-classical quantum superpositions of distinct waves only in a *conditional* fashion<sup>12,13</sup>. Here we experimentally demonstrate the *deterministic* conversion of a

**single-photon state into a quantum superposition of two weak coherent states with opposite phases – a Schrödinger kitten state<sup>12,13</sup> – and back. Conceptually different from all previous experiments, as being fully reversible, this can be interpreted as a quantum gate, connecting the complementary regimes of particle-like and wave-like light fields in a unitary fashion, like in a quantum computation. Such an unconditional conversion is achieved by means of a squeezing operation, demonstrating a fundamental feature of any quantum system: particle-like and wave-like properties can be reversibly altered, with no need for filtering out either through detection<sup>14</sup>.**

The prime example for Bohr’s complementarity principle<sup>1</sup> is wave-particle duality. It has been observed in double-slit experiments<sup>2</sup>, both for massive particles<sup>3,4</sup> and for particles without mass<sup>5,6</sup>. In general, the essence of duality is that, depending on a given experimental situation, detection of a quantum system may either reveal which-path information (the system unambiguously passes through one of the two slits – like a particle) or it may not (the system simultaneously propagates through both slits creating two interfering elementary systems – like a wave). Although all quantum states of light can potentially show both the “particle-like” and the “wave-like” behavior, some states are more particle-like, while others are more wave-like. One of the most particle-like states of light is the single-photon state  $|1\rangle$ . This is a highly non-classical energy eigenstate of a quantized oscillator with a totally undetermined phase. Typical optical duality experiments observe transitions from this most particle-like state to more wave-like states such as  $|1,0\rangle + |0,1\rangle$  using linear interference of two optical paths. Conversely, the most wave-like state is that of ordinary laser light, i.e., a coherent state  $|\alpha\rangle$ . Unlike the single-photon state, a coherent state is composed of potentially infinitely many photons arranged in such a way that coherent states correspond to the quantum versions of classical light waves with amplitudes  $\alpha = |\alpha|e^{i\theta}$  (ref. 11).

The close-to-classical nature of coherent states means their properties are easily simulated classically, for instance, with help of non-negative probability distributions. As a consequence, such states are of limited use in general quantum information processing where highly non-classical features are required<sup>9,15</sup>. Therefore, we shall focus on the coherent-state superposition (CSS),  $|\alpha\rangle - |-\alpha\rangle$ , which is indeed a highly non-classical state sufficient for universal quantum computation<sup>16</sup>. In the following, we demonstrate that a single-photon state can be unconditionally transformed into a CSS – an operation that so far has been realized only probabilistically<sup>17</sup>. Further, our experiment shows that the same operation transforms a CSS back into a single photon. In other words, our experiment demonstrates an unconditional and reversible two-way conversion between a single quantum particle and a non-classical, continuous wave. The action of this conversion is measurement-free, entirely independent of a (possibly delayed) detector choice.

The ideal quantum optical states in Fig. 1 serve as an illustration for those states occurring in our experiment. Recall that wave and particle properties in quantum optics are formally connected via a pair of annihilation and creation operators for photons,  $\hat{a}$  and  $\hat{a}^\dagger$ , respectively. These non-Hermitian operators are the quantized versions of the complex and complex conjugate amplitudes of an optical field mode, satisfying the bosonic commutation relation  $[\hat{a}, \hat{a}^\dagger] = 1$ . Similarly, the quadrature operators,  $\hat{x} = (\hat{a} + \hat{a}^\dagger)/\sqrt{2}$  and  $\hat{p} = (\hat{a} - \hat{a}^\dagger)/i\sqrt{2}$ , correspond to the quantized real and imaginary parts of the optical complex amplitudes (up to a factor  $\sqrt{2}$ ), where  $[\hat{x}, \hat{p}] = i$ . Through homodyne detection, the quadrature  $\hat{x}(\theta)$  can be measured, which gives an Hermitian part of the operator  $\hat{a}e^{-i\theta}$ ;  $\theta = 0$  and  $\theta = \pi/2$  then correspond to  $\hat{x}$  and  $\hat{p}$ , respectively.

In Fig. 1, the phase-dependent quadrature distributions are shown for a single-photon state, a CSS, and two coherent states. Any coherent state is an eigenstate of the annihilation operator,  $\hat{a}|\alpha\rangle = \alpha|\alpha\rangle$ . In Fig. 1, this corresponds to a sinusoidal wave with mean complex amplitude  $\alpha$

and minimal quantum noise<sup>11</sup>. By superimposing two coherent states,  $|\alpha\rangle - |-\alpha\rangle$ , the quadrature distribution corresponds to two sinusoidal waveforms with quantum interference at each intersection. This quantum interference is a witness of the quantum superposition of  $|\alpha\rangle$  and  $|-\alpha\rangle$  and it would never occur for a stochastic mixture of coherent states.

We perform the conversion from single-photon state (Fig. 1a) to CSS (Fig. 1b) by means of a squeezing operation,  $\hat{S}(\gamma) = e^{\gamma(\hat{a}^\dagger 2 - \hat{a}^2)/2}$ , where  $\gamma \in \mathbb{R}$  quantifies the amount of squeezing. In the particle picture, the effect of the squeezing is an infinite superposition of photons added and subtracted in multiples of two. As a result, squeezing leads to a superposition of even photon number states when applied to the vacuum and to a superposition of odd photon number states when applied to the single-photon state. Being in such an odd-number superposition is also a distinct feature of the target CSS,

$$|\alpha\rangle - |-\alpha\rangle \propto |1\rangle + \frac{\alpha^2}{\sqrt{6}} |3\rangle, \quad (1)$$

and this is exactly the reason why squeezing achieves the desired conversion<sup>18</sup>. For a description of our conversion in the wave picture, we refer to the supplementary information.

The schematic of our experimental setup is shown in Fig. 2. In order to verify the conversions, we perform quantum homodyne tomography on input and output states<sup>19,20</sup>. The experimental results for converting single-photon states into several CSSs are shown in Fig. 3, and those for the reciprocal conversion are given in Fig. 4. The top panel of each figure shows quadrature distributions obtained by a series of homodyne measurements, similar to the ideal states in Fig. 1. From these, Wigner functions and photon-number density matrices are calculated, as shown in the lower panels. Here, the diagonal elements of the density matrices represent photon number distributions, while the off-diagonal elements correspond to superpositions of  $|1\rangle$  and  $|3\rangle$ . In Fig. 3, the leftmost column shows the input single-photon state, and the right three columns show the output CSSs with three different squeezing levels,  $\gamma = 0.26$ , 0.37, and 0.67, corresponding to three different amplitudes of CSSs,  $\alpha = 0.91$ , 1.10, and 1.64,

respectively. In Fig. 4, the left column shows the input CSS with  $\alpha = 0.97$ , and the right column shows the output single-photon state obtained through squeezing with  $\gamma = -0.26$ .

Using Figs. 3 (for  $|1\rangle \rightarrow \text{CSS}$ ) and 4 (for  $\text{CSS} \rightarrow |1\rangle$ ), we shall discuss the quadrature distributions (top panels), the Wigner functions (middle panels), and the density matrices (bottom panels) of the experimental states before and after conversion. The phase-independent input quadrature distribution in Fig. 3 closely resembles that of the ideal single-photon state in Fig. 1a. Through squeezing, the quadrature distribution is turned into two opposite sine waves with quantum interference, which agrees well with the distribution for an ideal CSS in Fig. 1b. The phase-dependent oscillations increase with larger squeezing. The gap at the intersection of the waves is a witness for the quantum interference between the waves. This gap becomes less pronounced for larger  $\gamma$  because of the finite squeezing of the ancilla mode (about 7 dB relative to shot noise). In Fig. 4, an input CSS is subject to conversion, resulting in a phase-independent distribution with a gap, like for a single-photon state. In the corresponding Wigner functions (where detector inefficiencies and losses are not corrected), the non-classicality of the input and output states becomes manifest in negative values. These Wigner functions are converted from rotationally symmetric to asymmetric (Fig. 3) and from asymmetric to symmetric (Fig. 4), while preserving their large negative values at the phase-space origin. The number density matrix representation for the input single-photon state in Fig. 3 has a dominant single-photon component of 84% (without any corrections), while the input CSS in Fig. 4 has dominating one- and three-photon components compared to the zero-, two-, and four-photon terms. This also holds for the off-diagonal interference terms such as  $|1\rangle\langle 3|$ . Two-photon creations and annihilations are revealed by an increase (Fig. 3) and a decrease (Fig. 4) of the three-photon components, respectively.

In order to quantitatively assess the experimental conversion processes, besides reconstructing the Wigner functions and density matrices of the input and output states, we used two

additional figures of merit. These are specifically designed to reveal either the most distinct features of the particle-to-wave transition or that of the converse, wave-to-particle transition<sup>21</sup> (for details, see supplementary information).

A fundamental element of quantum theory is duality: the simultaneous presence of particle-like and wave-like features in any quantum system. More mathematically, in Hilbert space, a given quantum state can be expressed in any basis. For instance, a single-photon state is a discrete number state and, at the same time, a continuous superposition of continuous-wave states. Our universal low-loss broadband squeezer is capable of deterministically manipulating such superpositions. Using it, we have demonstrated unconditional two-way conversions between particles and waves, i.e., between continuous and discrete superpositions of waves. This is achieved entirely on the quantum level by means of a measurement-free, unitary, reversible map in Hilbert space – the squeezing operation. With this operation we have, for the very first time, access to a complete set of deterministic Gaussian operations applicable to non-classical, non-Gaussian states. These expand the toolbox for hybrid quantum information processing<sup>14</sup>, and therefore our result will directly lead to applications in this area.

## METHODS SUMMARY

The schematic of our experimental setup is shown in Fig. 2. It consists of two parts: a source of non-classical states and an unconditional squeezer. For the former, via a small variation of the setup, we can choose the non-classical states to be either a single photon or a CSS. The states will always emerge randomly in time, however, from a photon “click” at the avalanche photodiode (APD), we know whenever a state arrives. These “heralded” non-classical states are localized in time around the detections of correlated photons<sup>13,22</sup>. Therefore, our unconditional squeezer must have enough bandwidth to be applicable in the corresponding short time slots<sup>8</sup>. We extended our previous measurement-based squeezer<sup>23</sup> to meet this requirement. This

squeezer avoids direct coupling of fragile input states to nonlinear optical media, which typically involves large optical losses. Instead, an ancillary squeezed state is utilized as a resource of nonlinearity<sup>24</sup> (see supplementary information). Although our squeezer is assisted by homodyne detection on the ancilla beam, the non-classical signal state is never directly measured (see the quantum eraser<sup>25</sup>) when the squeezer is applied.

---

- [1] Bohr, N. Quantum postulate and recent developments in atomism. *Naturwissenschaften* **16**, 245–257 (1928); The quantum postulate and the recent development of atomic theory. *Nature (London)* **121**, 580–590 (1928).
- [2] Messiah, A. *Quantum Mechanics* (North-Holland Publishing Company, Amsterdam, 1961).
- [3] Jönsson, C. Electron diffraction at multiple slits. *Am. J. Phys.* **42**, 4–11 (1974).
- [4] Tonomura, A., Endo, J., Matsuda, T., Kawasaki, T. & Ezawa, H. Demonstration of single-electron buildup of an interference pattern. *Am. J. Phys.* **57**, 117–120 (1989).
- [5] Scully, M. O., Englert, B.-G. & Walther, H. Quantum optical tests of complementarity. *Nature (London)* **351**, 111–116 (1991).
- [6] Bertet, P. *et al.* A complementarity experiment with an interferometer at the quantum-classical boundary. *Nature (London)* **411**, 166–170 (2001).
- [7] Duan, L. M., Lukin, M. D., Cirac, J. I. & Zoller, P. Long-distance quantum communication with atomic ensembles and linear optics. *Nature (London)* **414**, 413–418 (2001).
- [8] Lee, N. *et al.* Teleportation of nonclassical wave packets of light. *Science* **332**, 330–333 (2011).
- [9] Lloyd, S. & Braunstein, S. L. Quantum computation over continuous variables. *Phys. Rev. Lett.* **82**, 1784 (1999).
- [10] Ionicioiu, R. & Terno, D. R. Proposal for a quantum delayed-choice experiment. *Phys. Rev. Lett.* **107**, 230406 (2011).
- [11] Glauber, R. J. Coherent and incoherent states of the radiation field. *Phys. Rev.* **131**, 2766–2788 (1963).

- [12] Ourjoumtsev, A., Tualle-Brouri, R., Laurat, J. & Grangier, P. Generating optical Schrödinger kittens for quantum information processing. *Science* **312**, 83–86 (2006).
- [13] Wakui, K., Takahashi, H., Furusawa, A. & Sasaki, M. Photon subtracted squeezed states generated with periodically poled KTiOPO<sub>4</sub>. *Opt. Exp.* **15**, 3568–3574 (2007).
- [14] Furusawa, A. & van Loock, P. *Quantum Teleportation and Entanglement: A Hybrid Approach to Optical Quantum Information Processing* (Wiley VCH, Berlin, 2011).
- [15] Bartlett, S. D., Sanders, B. C., Braunstein, S. L. & Nemoto, K. Efficient classical simulation of continuous variable quantum information processes. *Phys. Rev. Lett.* **88**, 097904 (2002).
- [16] Ralph, T. C., Gilchrist, A., Milburn, G. J., Munro, W. J. & Glancy, S. Quantum computation with optical coherent states. *Phys. Rev. A* **68**, 042319 (2003).
- [17] Ourjoumtsev, A., Jeong, H., Tualle-Brouri, R. & Grangier, P. Generation of optical ‘Schrödinger cats’ from photon number states. *Nature (London)* **448**, 784–786 (2007).
- [18] Lund, A. P., Jeong, H., Ralph, T. C. & Kim, M. S. Conditional production of superpositions of coherent states with inefficient photon detection. *Phys. Rev. A* **70**, 020101(R) (2004).
- [19] Lvovsky, A. I. & Raymer, M. G. Continuous-variable optical quantum-state tomography. *Rev. Mod. Phys.* **81**, 299–332 (2009).
- [20] Lvovsky, A. I. Iterative maximum-likelihood reconstruction in quantum homodyne tomography. *J. Opt. B* **6**, S556–S559 (2004).
- [21] Grangier, P., Roger, G. & Aspect, A. Experimental evidence for a photon anticorrelation effect on a beam splitter: a new light on single-photon interference. *Europhys. Lett.* **1**, 173–179 (1986).
- [22] Neergaard-Nielsen, J. S., Melholt Nielsen, B., Takahashi, H., Vistnes, A. I. & Polzik, E. S. High purity bright single photon source. *Opt. Exp.* **15**, 7940–7949 (2007).
- [23] Yoshikawa, J. *et al.* Demonstration of deterministic and high fidelity squeezing of quantum information. *Phys. Rev. A* **76**, 060301(R) (2007).
- [24] Filip, R., Marek, P. & Andersen, U. L. Measurement-induced continuous-variable quantum interactions. *Phys. Rev. A* **71**, 042308 (2005).
- [25] Andersen, U. L., Glöckl, O., Lorenz, S., Leuchs, G. & Filip, R. Experimental demonstration of continuous variable quantum erasing. *Phys. Rev. Lett.* **93**, 100403 (2004).

**Acknowledgements** This work was partly supported by PDIS, GIA, G-COE, APSA and FIRST commissioned by the MEXT of Japan, SCOPE program of the MIC of Japan, and, JSPS and ASCR under the Japan-Czech Republic Research Cooperative Program. R.F. acknowledges projects P205/12/0577 of GA ČR. P.M. acknowledges Post-doc project GPP205/10/P319 of GA ČR.

**Author Contributions** Experiments were performed by Y.M., J.Y., N.I., M.E., advised by A.F., where Y.M. was a primary workforce of the whole experiment, J.Y. contributed to the squeezer part, N.I. contributed to generation of a high-fidelity single-photon state, and N.I. and M.E. contributed to its squeezing. The discussion of the results and preparation of the manuscript were done by Y.M., J.Y., P.M., R.F., P.vL., A.F.; especially, P.M. and R.F. largely contributed to the evaluation of the CSS in the supplementary discussions.

**Author Information** Correspondence and requests for materials should be addressed to A.F. (akiraf@ap.t.u-tokyo.ac.jp).

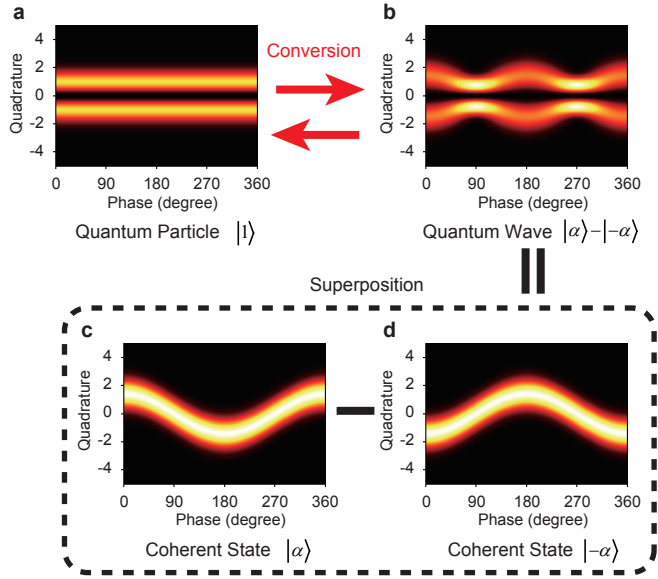


Figure 1: **Theoretical quadrature-distributions of four quantum states.** **a**, a single-photon state  $|1\rangle$ , **b**, a superposition of coherent states  $|\alpha\rangle - |-\alpha\rangle$ , **c**, **d**, two opposite coherent states  $|\pm\alpha\rangle$ , with the complex amplitude of  $\alpha = 1$ . Brighter color represents higher probability.

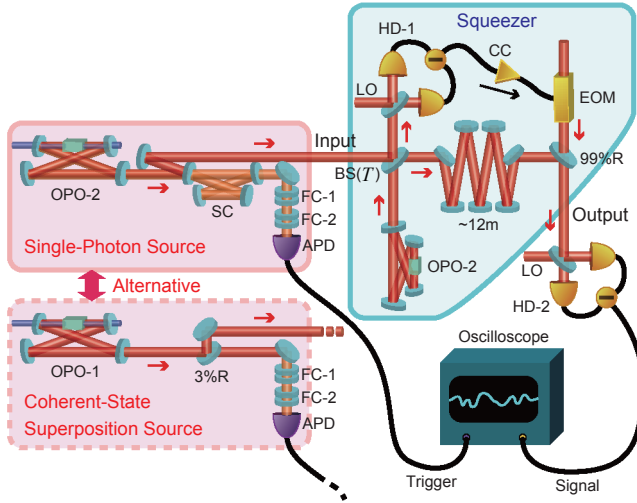
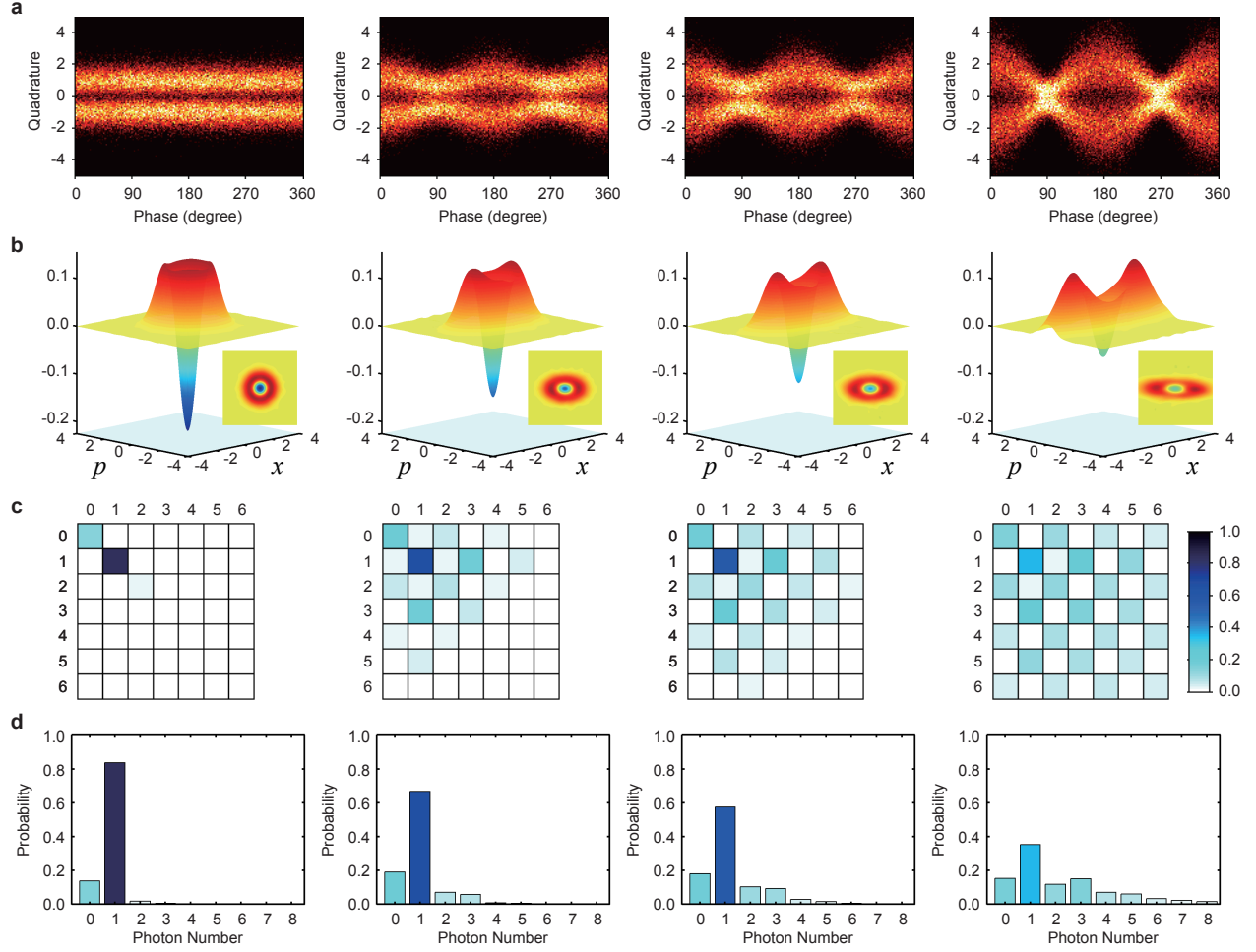


Figure 2: **Experimental setup.** BS( $T'$ ): beam splitter with transmittance  $T$  determining the degree of squeezing, OPO: optical parametric oscillator, SC: separating cavity, FC: filter cavity, APD: avalanche photo diode, HD: homodyne detector, LO: optical local oscillator, EOM: electro-optic modulator, CC: classical channel, R: reflectivity. An optical delay line of about 12 m is used to match the propagation times of the two signals, one of which gets converted to an electrical signal and back, while the other one remains optical throughout.



**Figure 3: Experimental quantum states for the conversion from particle to wave.** The leftmost column shows the input single-photon state, while the other three columns show the output states for a squeezing parameter  $\gamma$  of 0.26, 0.37, and 0.67, from left to right. **a**, quadrature distributions over a period, **b**, Wigner functions, **c**, photon number representation of density matrices, **d**, photon number distributions, corresponding to the diagonal elements of the density matrices. The minimum value of  $-0.22$  for the input Wigner function becomes, respectively,  $-0.15$ ,  $-0.12$ , and  $-0.06$ , after the conversion.

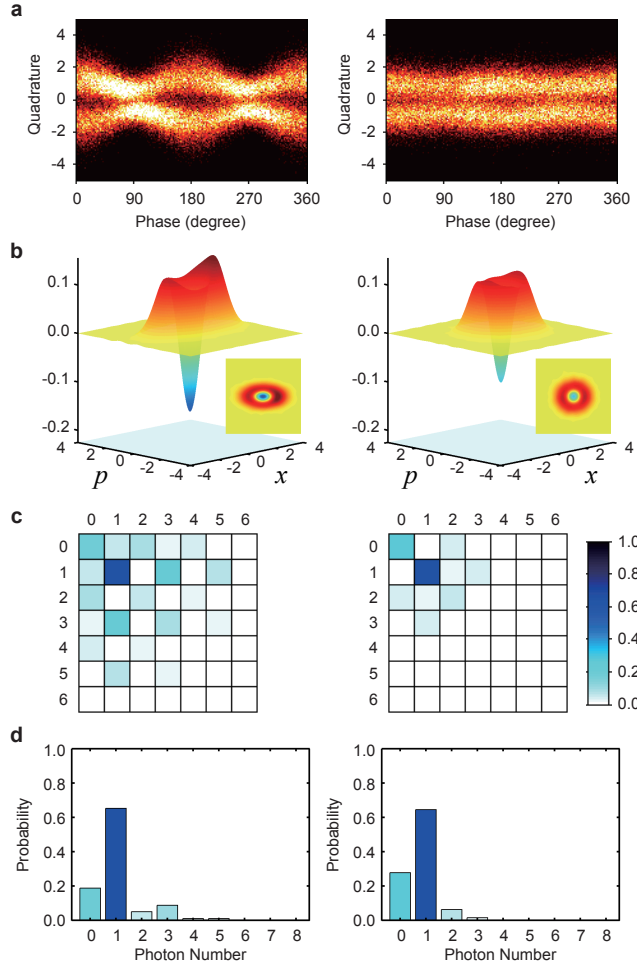


Figure 4: **Experimental quantum states for the conversion from wave to particle.** The left column shows the input coherent-state superposition and the right column shows output single-photon state. The squeezing parameter  $\gamma$  is  $-0.26$ . **a**, quadrature distributions over a period, **b**, Wigner functions, **c**, photon number representation of density matrices, **d**, photon number distributions, corresponding to the diagonal elements of the density matrices. The minimum value of  $-0.16$  of the input Wigner function is well preserved at the output with  $-0.10$ .

## Supplementary Information

### I. SUPPLEMENTARY DISCUSSION

**Conversion in Wave Picture** – In the wave picture, squeezing acts on the single photon state as a phase-sensitive amplifier, amplifying one quadrature ( $\hat{x}$ ) while noiselessly damping (squeezing) the other one ( $\hat{p}$ ). Now notice that, due to duality, the single-photon state can be recast as a *continuous* superposition of CSSs with all possible phases,  $|1\rangle \propto \int (|\alpha e^{i\phi}\rangle - |-\alpha e^{i\phi}\rangle) d\phi$ . The squeezing then drives the coefficients of the CSSs towards the states  $|\alpha\rangle$  and  $|-\alpha\rangle$ , and we obtain a *discrete* superposition,  $\hat{S}(\gamma)|1\rangle \approx |\alpha\rangle - |-\alpha\rangle$ , especially when  $|\alpha| < 1.2$ , with an approximation error less than 1%<sup>18</sup>. By inverting the unitary squeezing, the CSSs are converted back into the single-photon state,  $\hat{S}(-\gamma)(|\alpha\rangle - |-\alpha\rangle) \propto |1\rangle$ , regaining their phase independence within the continuous superposition forming  $|1\rangle$ .

**Conversion Criteria** – In order to quantitatively assess the transition between particle-like and wave-like states we employ the following figures of merit. First, note that the ideal initial and target states, the Fock state  $|1\rangle$  and the coherent-state superposition  $|\text{CSS}_{\text{id}}(\alpha)\rangle \propto |\alpha\rangle - |-\alpha\rangle \propto |1\rangle + \alpha^2|3\rangle/\sqrt{6}$ , become identical when  $\alpha \rightarrow 0$ . Hence the usual measure of fidelity between the experimentally generated states and an ideal state  $|\psi\rangle$ ,  $F = \langle\psi|\rho|\psi\rangle$ , is not a useful figure of merit. For example, the overlap between the experimental  $\rho$  and a target CSS,  $F(\alpha) = \langle\text{CSS}_{\text{id}}(\alpha)|\rho|\text{CSS}_{\text{id}}(\alpha)\rangle$  would optimally attain a value close to the maximal value of unity. This can be achieved when the state  $\rho$  approaches an ideal CSS with amplitude  $\alpha$ , but also when  $\rho$  is close to  $|1\rangle$  for  $\alpha \rightarrow 0$ . In order to avoid such a confusion between our particle-like and wave-like states and to gain a better insight into each generated state's properties, we divide the fidelity into two separate measures: the coherent-state distinguishability factor,  $D(\beta) = (\langle\beta|\rho|\beta\rangle + \langle-\beta|\rho|-\beta\rangle)/2$ , and the coherent-state interference factor,

$$V(\beta) = (\langle \beta | \rho | -\beta \rangle + \langle -\beta | \rho | \beta \rangle) / 2.$$

Here,  $D(\beta)$  describes the average overlap of the investigated state  $\rho$  with an independent pair of coherent states with amplitudes  $\pm\beta$ , which form the ideal superposition. When  $\beta = 0$ , this overlap vanishes for our odd-number CSS, while it would become unity for an even-number CSS,  $|\alpha\rangle + |-\alpha\rangle$ . In either case, as well as for an incoherent mixture of coherent states  $|\pm\alpha\rangle$ ,  $D(\beta)$  has, ideally, two separated symmetric peaks with maxima approaching 0.5 when  $|\alpha| > 2$ . On the other hand, the single-photon state  $|1\rangle$  has a maximal distinguishability  $D_1^{max} = 0.37$  at  $\beta \approx 1$ . An additional feature separating the CSS from the single-photon state is that the distinguishability of  $|1\rangle$  is phase-insensitive,  $D_1(\beta e^{i\phi}) \equiv D_1(\beta)$ , whereas for both the ideal and the experimentally generated CSSs, it is not, having a maximum at  $\phi = 0$ .

Besides two separated coherent-state peaks in phase space, a CSS is characterized by interference between the coherent states. For the Wigner function, this interference gives a negativity at the phase-space origin. However, a single-photon state exhibits the same feature, and if we want to distinguish a CSS from a single-photon state, we must evaluate the difference in this interference. For this purpose, we introduce the interference factor  $V(\beta)$ , which is always positive for a balanced mixture of coherent states and always negative for both the single-photon and the CSS  $|\alpha\rangle - |-\alpha\rangle$ . This makes it useful for demonstrating nonclassical interference effects. However, this figure of merit achieves more. While it has a clear minimum for the single-photon state,  $V_1^{min} = -D_1^{max}$  at  $\beta = 0.97$ , for the ideal CSS, the position of the extreme depends on its amplitude and its value monotonically decreases to  $-0.5$  as  $\alpha$  increases. Although both for the ideal single-photon state and the ideal CSS, the distinguishability and the interference are related by  $D(\beta) = -V(\beta)$ , in the presence of realistic noise, this symmetry relation is broken and we benefit from treating the two quantities independently. Two benchmarks can be derived to demonstrate that we observe nontrivial interference effects in comparison to the classical theory. The first benchmark represents the interference achievable purely by a mixture of coherent

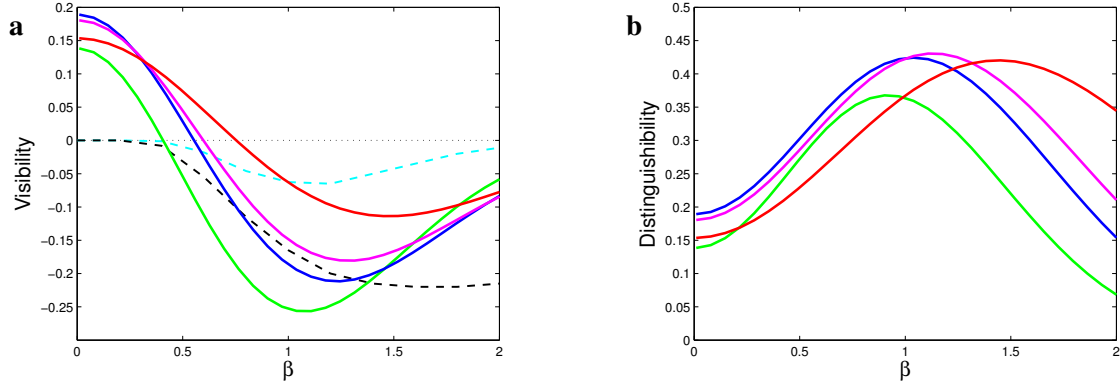
states. Passing it is a first witness of non-classical interference. Passing the second benchmark, obtained through optimization over all possible mixtures of Gaussian states, then serves as a witness of higher-order non-classical interference. Once again we stress that these criteria are different from simply observing negativities, which is always a witness of non-classicality, but does not discriminate between a CSS and a single-photon state like our interference factor  $V(\beta)$  does. In order to verify the particle-to-wave transition in our experiment, we employ  $D(\beta)$  in order to describe the emergence of the two coherent-state peaks in the CSS. At the same time,  $V(\beta)$  enables us to rule out incoherent mixtures and verify the presence of non-classical interference.

For the wave-to-particle transition, we introduce an additional figure of merit, since any loss of phase properties in  $D(\beta)$  and  $V(\beta)$  (as a possible indication for a successful conversion into a single-photon state) may as well be explained by an incoherent dephasing. In order to describe this reverse transition from the CSS back to the single-photon state, we take advantage of an important feature of the ideal single-photon state – it is indivisible at a beam splitter. This property, which has been essential in many single-photon experiments, can be evaluated through the so-called anti-correlation factor  $A^{21}$ . This operational measure is obtained assuming that the state in question is split at a balanced beam splitter and the two output modes are measured by realistic single-photon detectors. The anti-correlation parameter is then  $A = p_c/p_s^2$ , where  $p_c$  is the probability for both detectors registering a photon, while  $p_s$  is the probability for only one detector registering a photon (independent of the other detector). For a mixture of a single-photon and a vacuum state,  $p|1\rangle\langle 1| + (1 - p)|0\rangle\langle 0|$ , the anti-correlation parameter is  $A = 0$ , while classical light always has  $A \geq 1$ . As the amplitude of the ideal odd CSS increases,  $A = 1 - [1 - 2 \cosh(|\alpha|^2/2)]^{-2}$  grows from zero, approaching unity. For the ideal squeezed single-photon state,  $A$  increases monotonously with the squeezing and for  $|\gamma| > 0.66$ ,  $A$  becomes larger than unity, thus confirming the loss of the single-photon character.

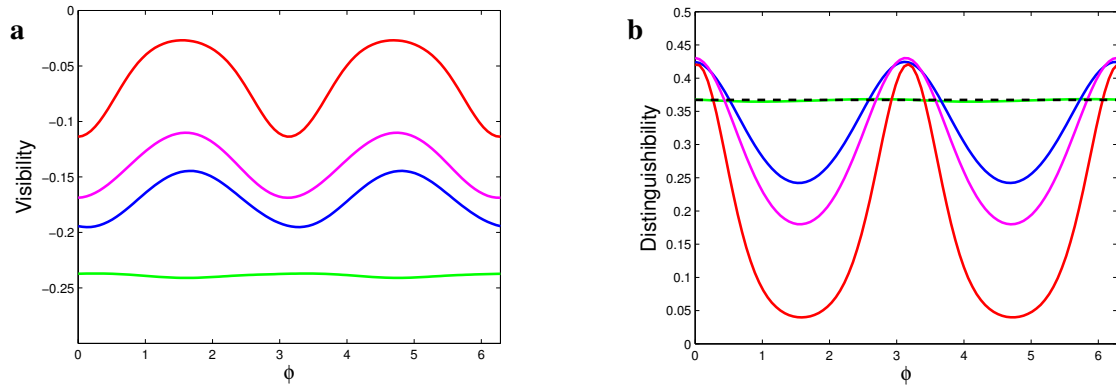
**Experimental Analysis** – The phase-insensitive superposition of coherent states present in a single-photon state,  $|1\rangle \propto \int(|\alpha e^{i\phi}\rangle - |-\alpha e^{i\phi}\rangle) d\phi$ , is a typical manifestation of wave-particle duality – even in the supposedly particle-like state  $|1\rangle$ , wave-like coherent states are present, but these form a continuous superposition with arbitrary phases and hence are not visible in the total state. However, in a  $|1\rangle \rightarrow \text{CSS}$  conversion, the squeezer can break this rotational symmetry and amplify coherent states along a single axis, thus making them more distinguishable while simultaneously preserving their interference features. This is demonstrated in Supp. Fig. 5, where we can see that squeezing not only increases distinguishability (which could as well be a consequence of Gaussian noise), but also shifts the maximum of  $D(\beta)$  towards larger values of  $\beta$ , as one would expect from a larger CSS. At the same time, the minimum of  $V(\beta)$  is also shifted, thus preserving the symmetry of an ideal CSS while remaining negative and distinct from a mixture of coherent states. The weakest squeezing operation ( $\gamma = 0.26$ ) even exhibits interference properties going beyond those of any Gaussian state. At the same time, in Supp. Fig. 6, we can observe a phase modulation of  $V(\beta)$  which emerges as a consequence of the phase-sensitive squeezing process.

For the opposite conversion,  $\text{CSS} \rightarrow |1\rangle$ , the above criteria are ambiguous, because the transitions of  $D(\alpha)$  and  $V(\alpha)$  and their loss of the phase dependence can be as well explained by an incoherent dephasing effect. However, by looking at the anti-correlation parameter  $A$ , which effectively serves as a measure of the ‘single-photon’ quality of the state, we see that the values of this parameter change from  $A_{\text{CSS}} = 0.52$  to  $A_{\text{SP}} = 0.29$ . Recalling that for an ideal single-photon state we have  $A = 0$ , this shows that the quality of the single-photon state present in the total state is enhanced, even though the absolute single-photon fraction in the resulting mixed state is actually reduced.

## II. SUPPLEMENTARY FIGURES



Supplementary Figure 5: Dependence of interference (visibility)  $V(\beta)$  and distinguishability  $D(\beta)$  on  $\beta$  for squeezing of a single-photon state. Solid lines: green - experimental single-photon state, blue - experimental squeezed single-photon state ( $\gamma = -0.38$ ), magenta - experimental squeezed single-photon state ( $\gamma = -0.50$ ), red - experimental squeezed single-photon state ( $\gamma = -0.72$ ). Dashed lines in **a**: black - bound for mixtures of Gaussian states, cyan - bound for mixtures of coherent states, dashed lines in **b**: black - single-photon state.



Supplementary Figure 6: Dependence of interference (visibility)  $V(\beta_0 e^{i\phi})$  and distinguishability  $D(\beta_0 e^{i\phi})$  on phase  $\phi$  for squeezing of a single-photon state. For each curve,  $\beta_0 \in \mathbb{R}$  was chosen as the point of the local extremum. For **a**: green - experimental single-photon state ( $\beta_0 = 1.11$ ), blue - experimental squeezed single-photon state ( $\gamma = -0.38, \beta_0 = 1.26$ ), magenta - experimental squeezed single-photon state ( $\gamma = -0.50, \beta_0 = 1.31$ ), red - experimental squeezed single-photon state ( $\gamma = -0.72, \beta_0 = 1.45$ ). **b**: green - experimental single-photon state ( $\beta_0 = 0.90$ ), blue - experimental squeezed single-photon state ( $\gamma = -0.38, \beta_0 = 1.04$ ), magenta - experimental squeezed single-photon state ( $\gamma = -0.50, \beta_0 = 1.11$ ), red - experimental squeezed single-photon state ( $\gamma = -0.72, \beta_0 = 1.45$ ). Dashed black - single-photon state ( $\beta_0 = 0.97$ ).

### III. SUPPLEMENTARY METHODS

As a fundamental light source, we utilize a continuous-wave Ti:sapphire laser with a wavelength of 860 nm. Some part of the fundamental wave is converted to a second harmonic wave in order to pump the optical parametric oscillators (OPO-1 and 2). As a non-classical input state, we generate single-photon states, or, alternatively, coherent-state superpositions (CSSs). In Fig. 2 of the main text, the setup for creating these input states is visualized by an orange background. Compared to the setups of refs. 13 and 22, in the present scheme, we can switch between the two different non-classical input states. In the case of a  $|1\rangle$  input, non-degenerate photon pairs are generated in OPO-1 and one photon of every pair is then detected by an avalanche photo diode (APD). A click of the APD at this arm heralds the presence of a single photon in the other arm. The separating cavity (SC) behind OPO-1 allows for a spatial separation of each pair of correlated photons. The filtering cavities (FCs) extract a single frequency mode of OPO-1 from hundreds of modes in every 590 MHz of the hundreds GHz bandwidth of quasi-phase-matching, where 590 MHz is the free spectral range of OPO-1. For the case of an initial CSS, OPO-1 generates degenerate photon pairs, i.e., squeezed vacuum states. Every click of the APD then corresponds to the subtraction of a photon i.e.,  $\hat{a}\hat{S}(\gamma)|0\rangle$ .

Our measurement-based squeezer works as follows (visualized by a blue background in Fig. 2 of the main text)<sup>24</sup>. An ancillary  $\hat{x}$ -squeezed state and the input quantum state are coupled by a beam splitter, where the level of squeezing  $\gamma$  can be adjusted by the beam-splitting ratio  $T$  with  $T = \exp(-2\gamma)$ . We demonstrate three different squeezing levels,  $\gamma = 0.26, 0.37$ , and  $0.67$ , corresponding to  $T = 0.59, 0.48$ , and  $0.26$ , respectively. Then, one output of the beam splitter is measured with respect to the  $\hat{p}$  quadrature and the outcome is fed forward to the other output mode. A negative squeezing parameter *e.g.*  $\gamma = -0.26$  is achieved by  $90^\circ$  rotations of the optical phases, corresponding to a  $\hat{p}$ -squeezed ancilla, a measurement with respect to  $\hat{x}$ , and a

feedforward on  $\hat{x}$ . The feedforward operation is performed as follows. First, a phase modulation is added to an auxiliary beam by means of an electro-optic modulator (EOM), where the applied voltage is proportional to the measurement result. Then, the auxiliary beam is coupled to the signal beam by a highly asymmetric beam splitter. An optical delay of 12 m is utilized for a broadband synchronization of the feedforward<sup>8</sup>. Thus, we achieve broadband squeezing of up to 10 MHz, which is 300 times broader than the conventional squeezing<sup>23</sup>. Note that the bandwidth limitation is that of the ancillary squeezed light. The bandwidth is broad enough to operate a full 6 MHz bandwidth of the heralded quantum states, where 6 MHz is the half-width-half-maximum of OPO-1.